CORROSION SCIENCE AND TECHNOLOGY, Vol.23, No.3(2024), pp.179~194 pISSN 1598-6462 / eISSN 2288-6524
[Research Paper] DOI: https://doi.org/10.14773/cst.2024.23.3.179

Assessment Corrosion and Bioactive Behavior of Bioglass Coating on Co-Cr-Mo Alloy By Electrophoretic Deposition For Biomedical Applications

Areege K. Abed†, Ali. M. Mustafa, and Ali M. Resen

Production Engineering and Metallurgy Department, University of Technology, Baghdad, Iraq
(Received February 23, 2024; Revised April 21, 2024; Accepted April 22, 2024)

A layer-by-layer coating was produced using electrophoretic deposition for a HA/Al_2O_3 coating layer and a bioglass coating layer on Co-Cr-Mo alloy with a roughness of 0.5 μm (400 emery paper SiC). The corrosion behaviour was analyzed by assessing the coating layers' exceptional corrosion resistance, which outperformed the substrate. Cr ion release test using AAS was carried out, indicating that factional graded coating inhibited ion release from the uncoated substrate to coated sample. The porosity was expressed as a percentage, representing the extent of imperfections on the surface of all coatings. These imperfections fell within an acceptable range of 1% to 3%. The roughness of the coated surface was measured using atomic force microscopy, which revealed an excellent roughness value of 3.32 nm. Tape test technique for adhesion revealed that the removal area of the substrate coating layer varied by 11.92%. X-ray diffraction analysis confirmed the presence of all coating material peaks and verified phases of the deposited coating layers. These findings provided evidence that the coating composition remains unaffected by the electrophoretic deposition process. The bioactivity was assessed by immersion in a simulated bodily fluid, which revealed the formation of HCA during a period of 5 days.

Keywords: *Electrophoretic deposition (EPD), Nano Alumina (Al_2O_3), Nano Hydroxyapatite (HA), Bioactive glass (BG)45S5*

1. Introduction

Tissue engineering field is exponentially growing due to the rising need of improving quality life of human beaning's. 316L stainless steel, Co-Cr-Mo alloys, and Ti-based alloys are examples of metallic biomaterials which are widely used as metallic implants, owing to their good mechanical properties and excellent biocompatibility [1,2].

In spite of these advantages, the metallic metallic implants need to be coated with bioactive materials to establish good interfacial bonds between the metal substrate and the bone bonding. bioactive material coating hydroxyapatite (HA) and bioactive glass (BG) were used in this approach. in recent years Bioactive glasses (BGs) become interesting alternatives to HAP for the production of prosthetic coatings [2,3]. Demonstrate the capacity to establish robust physical and chemical connections with soft and hard biological tissue [3,4]. Hench *et al.* introduced the first BG during the late 1960s. The BG, type 45S5 Bioglass, belongs to the Na_2O-CaO-P_2O_5-SiO_2 system. It consists of components naturally found in the human body, with a particular abundance of Ca and P in bone tissue. This composition makes BG 45S5 very suitable for bone regeneration purposes. The process involves the formation of hydroxycarbonate apatite, which is the mineral phase found in bone [5,6].

Nevertheless, bioactive glasses (BGs) are often unsuitable for load-bearing applications, such as the replacement of big bones. Thus, creating metal implants covered in glass ceramics and bio-glasses (BGs) is a commonly used technique in orthopedic applications. Combining the high mechanical capabilities of metal alloys with the bone-bonding capacity of BGs is an advantageous result [4,7].

In this study deposition conditions of bioglass were taken depending on the Tachuqi design of the experiment (DOE) the approach was applied for the first time along with gray relations analysis [5,8].

The functionally graded coating was achieved by deposit of BG with 2 layers, the first one has directly attached to the substrate and the second one should be

†Corresponding author: Pme.19.14@grad.uotechnology.edu.iq

attached to (SBF) or the human body, and mediated layer is (HA/Al_2O_3) composite.

It should be noted that the biocompatibility of alumina (Al_2O_3) is well proved through in vitro and in vivo tests such as cytotoxicity, sensitization, implantation, and genotoxicity, in animals and humans, it did not reveal any abnormal biological response [6,9]. Moreover, nanoparticles is less toxic nanomaterials then TiO_2, and SiO_2 [7,10]. Alumina has exceptional stability inside the human body, which might be ascribed to its remarkable chemical stability. Alumina is insoluble in both strong acids and strong bases [8,11].

The motivation behind using (HA/Al_2O_3) composite is to compensate for the shortage of BG mechanical properties and develping functionall graded coating (BG-composite-BG) on Co-Cr-Mo alloy through the electrophoretic deposition (EPD) technique. The influence of composite layer which contain (HA/Al_2O_3). on the behavior of the coating was studied, as the effect EPD parameters, coating thickness, adhesion strength, roughness, wetablity, antibecterial activity, The corrosion resistance of the composite coatings in simulated bodily fluid (SBF) and the release of ions were assessed.

2. Materials

The anode (counter electrode) and cathode (substrate electrodes) were employed of the same alloy (Co-Cr-Mo). Co-Cr-Mo alloy has a chemical composition showed in Table 1, the material the used in the work, first is binder material utilized in this study was chitosan, which was bought from Sigma Aldrich mix with chitosan had a medium molecular weight and a degree of deacetylation of about 85%. It was soluble in 1% acetic acid [12]. That dissolved in Acetic acid having a purity level greater than 98%. Than the solvents used are pure ethanol with a purity of 99.9% , the electrolyte consists of a mixture of water and ethanol, than the hydroxyapatite (reagent grade, powder, synthetic) (30 to100 nm, purity of 99%, white color with 3.140 g/cm^3 density) purchased from Sigma Aldrich was used to deposit it as a coating layer and the Nano Al_2O_3 (alumina) type Alfa with (30-5 nm) particle size, white color and purity of 99.99% and the Bioglass® 45S5 powder with a nominal composition of $45SiO_2$–$24.5Na_2O$–$24.5CaO$–$6P_2O_5$ (wt%)was used [5].

Table 1. Shows the chemical composition for alloy and its standard

NO.	Elements	Used alloy	ASTM F75 Required
1	Cobalt, Co	64.8%	Balance
2	Chromium, Cr	28.5%	27 – 30%
3	Molybdenum, Mo	5.3%	5 – 7%
4	Carbon, C	0.4%	< 0.35%
5	Silicone, Si	0.5%	< 1%
6	Manganese, Mn	0.5%	< 1%

3. Experimental method

3.1 Solution preparation

Because the types of solutions have high effects on properties and specifications of achieving the required results, Preparing the suspension needs high accuracy. This step included the preparation of two suspensions: the first one is composite (hydroxyapatite + alumina) (HA + Al_2O_3). Chitosan (0.5 g/L) was dissolved in 1% acetic acid [9] After that, the dissolve chitosan was added to the solution of a mixture of 94% ethanol + 5% deionized water. 5%C Al_2O_3 folloed by and 3%C HA was added, and the second one is to deposit BG, the solution preparation and deposition condition was taken depended on previous experiments. Magnetic stirring was used to deagglomerate all suspensions for 24 hours. Subsequently, a vigorous attorney (Ultrasonic Processor, MIXSONIX Incorporated, New York, USA) was used for 30 minutes. The pH value was determined 4 pH.

Initially, the alloy was cut using wire-cut to use as substrates with 10 × 10 × 1 mm dimensions to prepare the samples for EPD coatings. Then surface grinding with (400) grit SiC paper. Grinding was used to obtain the best surface roughness to enhance the adhesion with the substrate. After finishing, the samples are polished by a cloth and using diamond paste for final finishing and to obtain a smooth surface. Finally, all the samples are cleaned by ultrasonic for 15 min in acetone and dried at room temperature before depositing.

3.2 Process of electrophoretic deposition

The experimental setup used in this work comprises a beaker containing a suspension, with two electrodes

submerged therein. Both anode and cathode were employed of the (Co-Cr-Mo) alloy. The distance between them is 1 cm. The anode and cathode were washed with acetone and then dried before being used. By immersing the electrode inside a 50 mL beaker filled with solution, the deposition was carried out. The deposition carried out at room temperature. Upon completion of the EPD process, the electrode that had been coated had to be removed from the solution. After completing the EPD process, the samples were dried in the atmosphere [13].

3.2.1 Optical microscopy and Scanning electron microscopy (SEM)

Optical microscopy is important to ensure that a sample can be viewed as clearly as possible and used for characterizing the coating morphology and measuring thickness coating layer. The microstructure and cross section of all samples were performed and tested by the same microscope to characterize morphology layers in addition to measure thickness of layers.

(SEM) is a powerful magnification tool used to provide topographical, morphological and compositional. Scanning Electron Microscope can detect and analyze surface fractures, provide information in microstructures and characterize the surface. An Energy Dispersive X-ray Spectrometry (EDS) detector combined with SEM was employed to detect the elemental distribution of the selected points/area in the SEM image. The cross-sectional microstructures as well as the distribution of different components of the deposited coatings were evaluated by scanning electron microscopy" (SEM).

3.2.2 Roughness Measurement

Roughness measurement device type used to measure the roughness of all coated samples (at the optimal condition) by using micrometer instrument. Each measurement was repeated three times to each sample and take the average of them.

3.2.3 Atomic force microscopy (AFM)

The surface nano roughness of coating layers was measured by atomic force microscopy (AFM). AFM is an advanced technique of studying properties of materials at an atomic scale and analyze surface morphology and roughness of the EPD films.

3.2.4 Porosity Measurement

Porosity of the sample at the optimal condition measurement. Porosities amount are estimated in surface optical images by using image J program for all samples of single and milt- layer coating.

3.2.5 Adhesion Measurements

There are three different ways to find the resistance of the coating layer to separate from the substrate and provide different adhesion analysis of the film: a pull-off test, cross-hatch test and scrape adhesion test. In pull-off test the adhesion testing most commonly the methods. A special tape for testing was firmly applied over the cross-hatch test area and removed quickly by pulling the tape back off of the test area to reveal the amount of coating lifted off by the test tape. The removable area was calculated by using ImageJ program.

3.3 Wettability (Contact Angle)

Wettability or hydrophobicity (contact Angle) Measurements The treated and untreated samples were subjected to contact angle measurements by using a CCD camera. The absorption of the deionized water volume of about 2 μL droplet in the sample was recorded at one frame per 5 seconds. Contact angle was then plotted against absorption time to show the dynamics of the water droplet absorption on the surface of the sample. Three replicates for each experimental condition were considered. By a computer software which was connected with the wettability instrument to determine the value of contact angle that was appeared on the computer screen.

4. Results and Discussion

4.1 Microstructure Analysis of BG coating

The optical microscope and SEM were used to study both the topography and thickness as shown in Fig. 3 and 4. It was found from observation that the coating is characterized by its dense, porous, homogeneity, and high thickness was achieved for BG under good deposition conditions. The first and the last coating layer was BG layer with (80 μm) thickness as illustrated in the Table 4 and shown in Fig. 3 deposited at 60 V, 90 sec and 10% C. this condition was taken depending on tachuqi design of the experiment (DOE) the approach was applied for

the first time along with gray relations analysis. Good coating properites homogenize, dense, porous, and high thickness are a result of many factor. Zeta potential is the primary determinant in the EPD process, as it influences the stability of the solution and the uniformity of coating layer deposition, making it a crucial parameter. The values in Table 2 represent the zeta potential of 80.44 mv and mobility of 6.17 for BG solutions used for depositing different layers at room temperature, as seen in Fig. 1. The highest zeta potential indicates the highest mobility of the solution, higher mobility value indicates greater suspension stability and higher deposition rate, Enabling the substrate to be covered entirely and coated uniformly in less time. Table 2 show the value of zeta potential and mobility in optimum conditions of BG with TEA.

Due to wide range of BG particles from (1 to 10) μm the large particles are dispersed in fine particle of BG matrix, The difference in the particle size give highly coating porous [10], as shown in SEM image Fig. 4. Generally, an increase in porosity has two main effects [11]: firstly, it enhances the development of tissue when the implant is placed in the body, and secondly, it reduces the strength of coating adhesion and increases the corrosion rate. Hence, it is essential to strike a balance between these conflicting impacts. A balance must be achieved between these contradictory forces. Nevertheless, we hypothesize that the coating's porous structure significantly alleviated the residual stresses.

Table 2. Value of zeta potential and mobility in optimum conditions

Suspension type	Zeta potential (mv)	Mobility	PH
BG with TEA	80.44	6.17	8.5

With regard to the factors that affect the possibility of obtaining high or low porosity, they are: The suspension properties (concentration, zeta potential of particles, their size distribution and type of the solvent used) and the important role is the particle size because that layer gives the highest value of porosity due to the bigger particle size [14,15]. Both the amounts and size of porosity was estimated in Fig. 5 and 6 respectively. The amounts of the porosity obtained by image analysis are shown in Table 5. The red color presented the porosities and can be seen in Fig. 4. where BG coating layer have given porosity (11.265%). Furthermore, the coating exhibited a wide range of open-pore diameters, ranging from a few nanometers to 11 μm as shown in Fig. 5.

The coating contained homogeneously distributed, interconnected open pores with irregular geometries. Essentially, the size and dispersion of the particles within the coating determine the size of the pores. Osteointegration of the coated implant with bone tissue depends on the pore size, volume, and interconnectivity [10,16]. Porous ceramics should have a bimodal distribution of pore sizes [10,17]. The minimum diameter of interconnected pores should be between 100 and 135 μm to guarantee bone ingrowth and fixation [13,18]. However, Migra-Moszkowicz *et al.* reported that micropores with sizes below 10 μm might promote osteoblasts' adhesion, spreading, and proliferation [15,19].

The tiny pores facilitate the adsorption of bone-inducing proteins and the easy movement of nutrients and other components of physiological fluids. They also enable ion exchange and bone formation. Furthermore, as stated by Bignon *et al.*, the presence of microporosity within the range of 0.3-2 μm facilitates the expansion of the

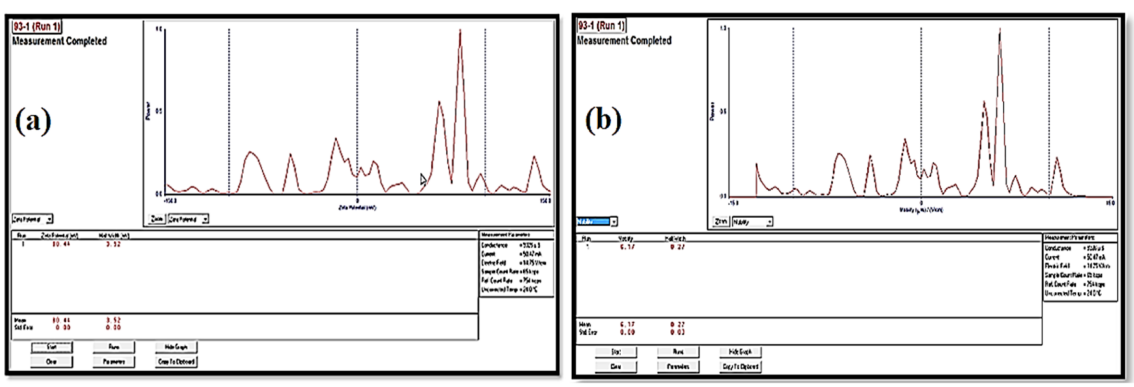

Fig. 1. Shows the (a) Zeta potential (b) Mobility measurements for different solutions of Bioglass with TEA

cytoplasm, hence promoting the spreading of cells [10,20]. The porosity of coatings is crucial since it directly affects the performance of implants. Because an open-pore structure is porous, it makes it easier for bone tissue to get into the coating. This improves bio integration and makes the implant more stable in the biological body. Thus, implant surfaces need pores to enable osteointegration [10,21].

4.2 Microstructure Analysis of Composite (HA/Al_2O_3) coating

Composite (HA/Al_2O_3) layer was the mideated coating layer, The optical microscope and SEM were used to study both the topography and thickness as shown in Fig. 4 and 5 .The thickness of this layer was (19 µm) thickness as illustrated in the Table 3 and shown in Fig. 4. deposited at (40 V, 1 min, 5%C Al_2O_3 0.5 g/L chitosan, and 3%C HA) this condition was taken depending on tachuqi design of the experiment (DOE). A zeta potential test was conducted to determine the solution's stability at PH equal to 4, and the result was a zeta potential value that was positive (70.45 mv) as well as the mobility value is (5.40), as indicated in Table 3, Fig. 2a and b This was the explanation for the solution's stability, demonstrating the coating layer's homogeneity and good thickness under these conditions. Due to the particle size of HA and Al_2O_3 used (30 to100 nm) and (30-5 nm) respectively, the porous size is very small as shown in Fig. 5b SEM images of topography for one-layer Composite ($HA+Al_2O_3$)

Table 3. Value of zeta potential and mobility in optimum conditions for Compo. deposition

Suspension type	Zeta potential (mv)	Mobility	PH
Compo. ($HA+ Al_2O_3$)	70.45	5.40	4

4.3 Microstructure Analysis of three-layer coating (BG+ Composite +BG)

The optical microscope and SEM shows the high thickness which up to (177 µm) and topography that similar to the ground layer. But we suppose that Because of the need for the large particles to acquire a greater surface charge than smaller one does to enable them to move towards the diposited electrode, with the passage of time and the increase in the thickness of the coating layers, it becomes difficult to deposit the large particles. Therefore, we note from Fig. 4c. Three layers (BG+ Composite +BG) that there are fewer number of large particles than that is in the Fig. 4a which represents one-layer of the BG. Therefore, this leads to reducing the difference in the size of the deposited particales. This explains the decrease in the Percentage value of porosities from 11.265 to 6.098 for one-layer BG and Three layer (BG+ Composite +BG) respectively as shown in the Table 5 and Fig. 5.

For confirmation purposes, the results of optical microstructure observations, SEM are used. Scanning electron microscopy coupled to EDX is used to identify the surface topography of samples after coatings. An SEM. EDS results in Fig. 7 indicate that there are no

Table 4. Thickness of coating layers at optimal condition

NO.	Type of sample	Thickness (µm) by Optical microscope
1	One-layer BG	80
2	One-layer Composite ($HA+Al_2O_3$)	19
3	Three layers (BG+ Composite +BG)	177

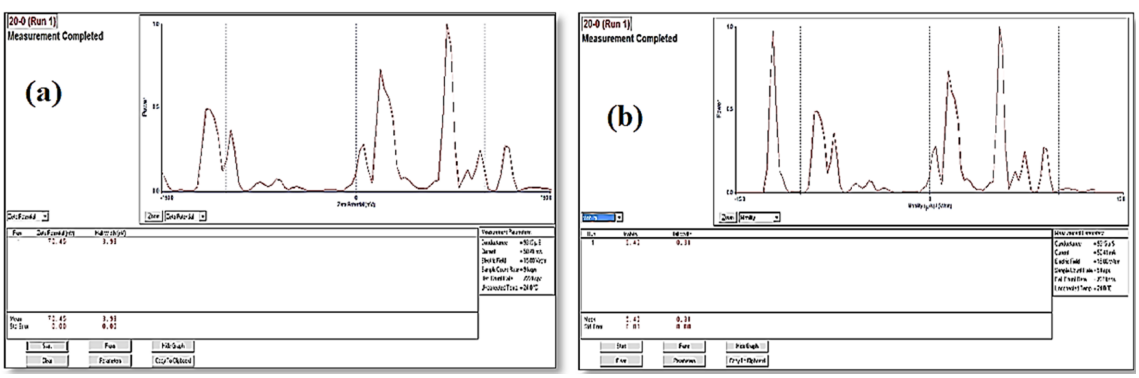

Fig. 2. (a) Zeta potential (b) Mobility measurements for composite suspension with optimum concentration (3% $HA+5\%Al_2O_3$)

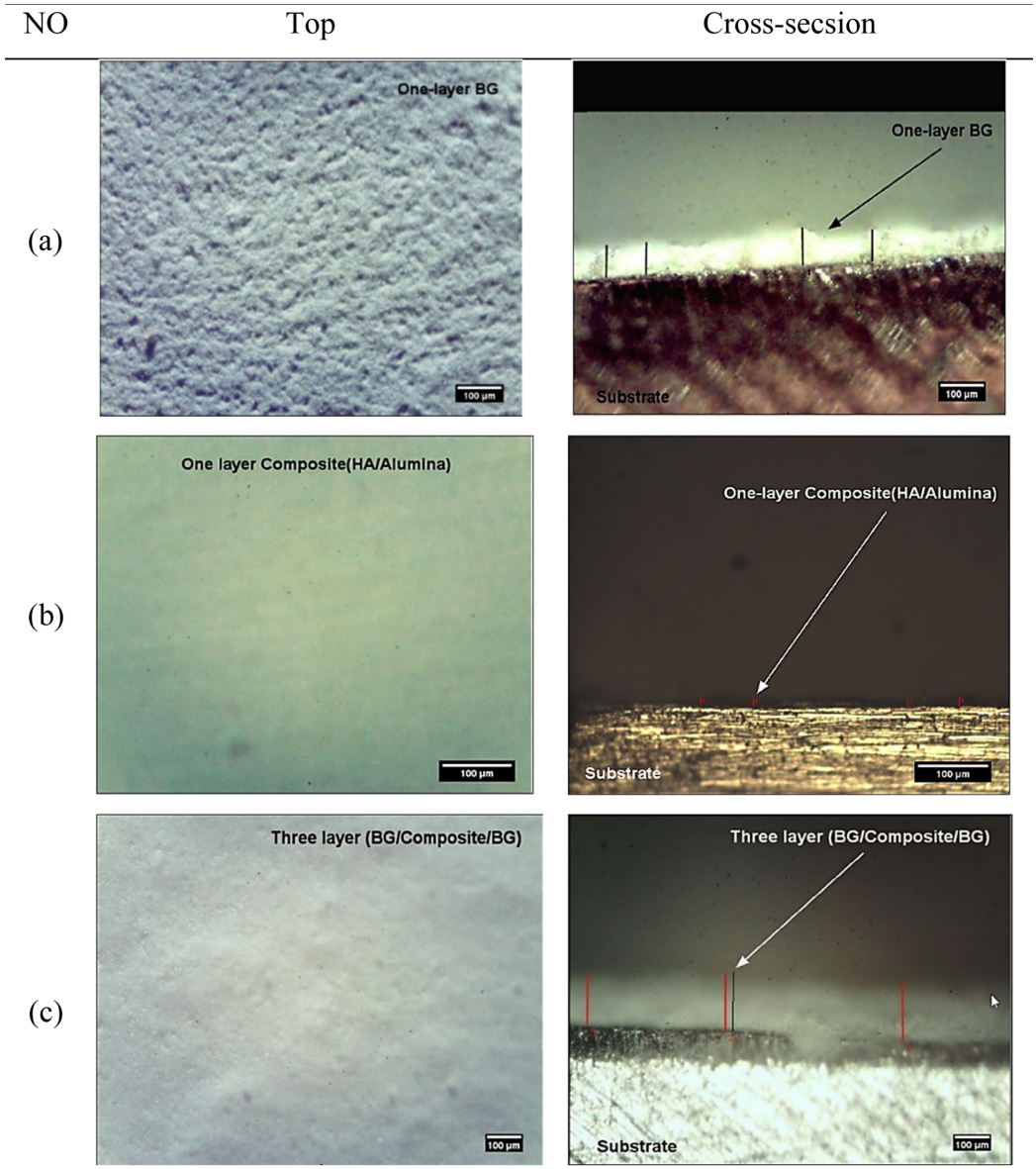

Fig. 3. Optical images of topography and cross section for (a) one-layer BG, (b) one-layer Composite (HA+ Al_2O_3), and (c) Three-layer (BG+ Composite +BG) coating samples

phases present other than hydroxyapatite (HA), aluminum oxide (Al_2O_3), chitosan and bioglass in the multi-layer coating sample (BG+ Composite +BG)

4.4 Roughness measurement

Nano roughness is measured by using the AFM technique as shown in Fig. 8. The Nano roughness of the coting sample was 2.91, 0.72, and 3.32 nm for one-layer BG, one-layer Composite (HA+ Al_2O_3) and Three layer (BG+ composite + BG) respectively.

The variation in roughness could be attributed to differences in HA particle size (100 nm), BG particle size (<10 µm), and alumina particle size (30-5 nm). Table 6 shows mean values of roughness for samples with an average diameter (nm) at the optimal conditions and

Table 5. Percentage value of porosities for coating layer

NO.	Type of sample	% Porosities
1	one-layer HA	2.056
2	one-layer BG	11.265
3	Three layers (BG+ Composite +BG)	6.098

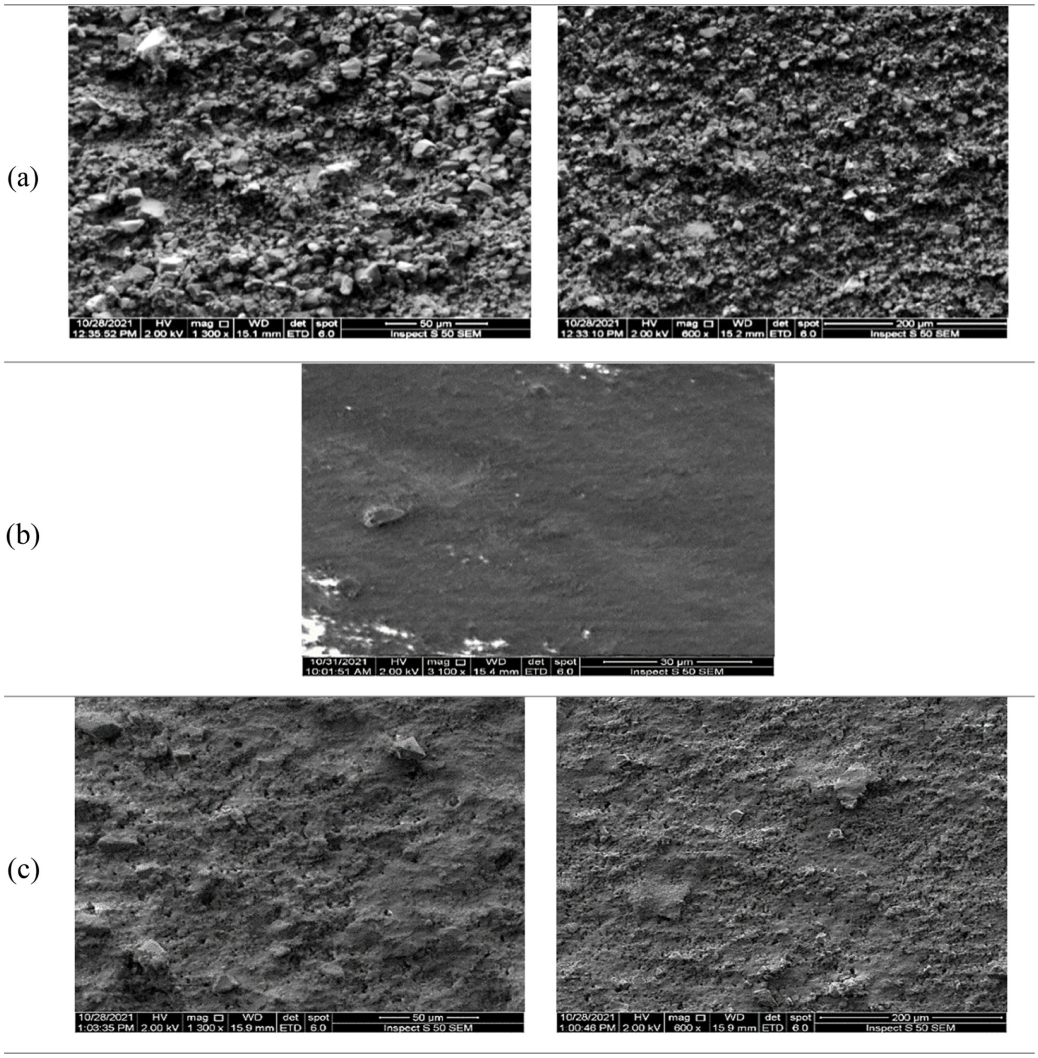

Fig. 4. SEM images of topography for (a) one-layer BG, (b) one-layer Composite ($HA+Al_2O_3$), and (c) Three-layer (BG+ Composite +BG) coating samples

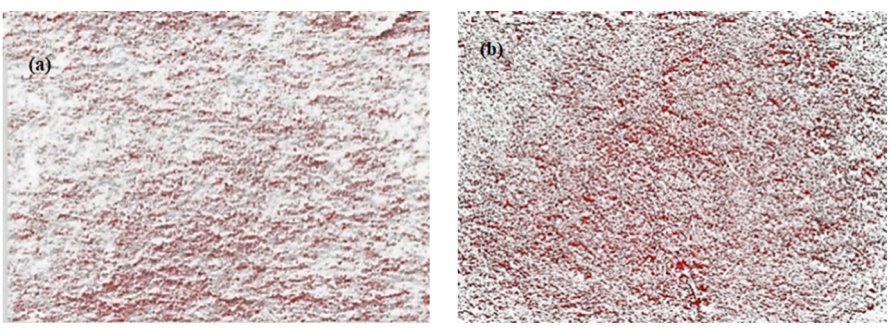

Fig. 5. Porosities estimation for (a) One-layer BG (b) Three-layer ($BG/AL_2O_3/BG$) coating samples.

different coating layers.

It should be pointed out that substrate roughness is a crucial aspect of the EPD process, particularly in bone replacement applications. A micrometer instrument is used for measuring roughness. The roughness on the implant's surface enhances adhesion, differentiation, and proliferation, resulting in a strong link between the implant and the host bone in the human body.

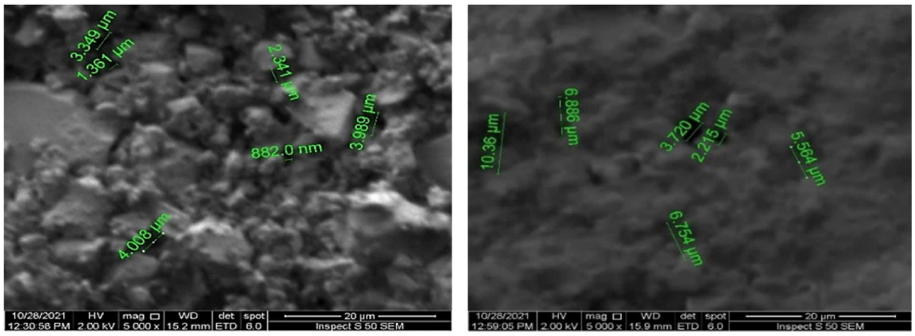

(a) (b)

Fig. 6. Porosities estimation for (a) One layer BG (b) Three-layer (BG/HA+AL$_2$O$_3$/BG) coating

Table 6. Shows mean values of roughness for samples at the optimal conditions

NO.	Type of sample	(Ra) nm	Average Diameter nm
1	one-layer BG	2.91	17.07
2	one-layer Composite (HA+Al_2O_3)	0.72	6.23
3	Three layers (BG+ Composite +BG)	3.32	34.71

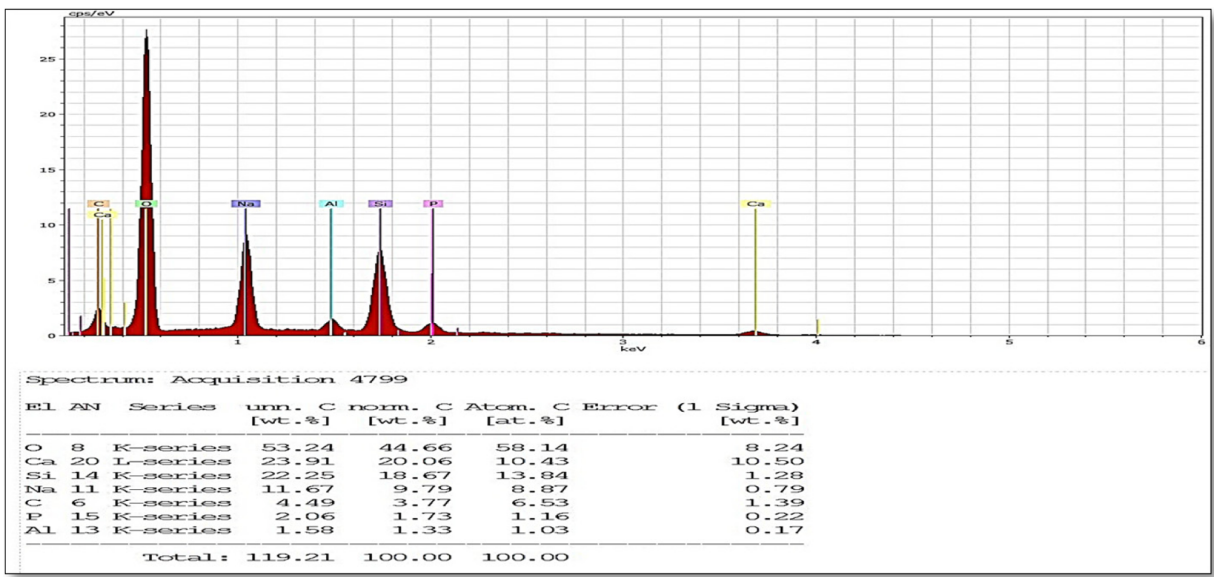

Fig. 7. EDS for three-layer (BG/AL$_2$O$_3$/BG) coating sample

4.5 Wettability (Contact angle)

The contact angle measurements are shown in Table 8. The surface wetness was assessed by measuring the contact angles using a sessile drop of distilled water placed on the sample surface. The contact angle of the uncoated Co-Cr-Mo sample is (60.19º), whereas the substrate with the coated with one-layer BG (6º), one-layer of composite (HA+Al_2O_3) (14º), and the three coating layers of (BG+ Composite +BG) have the lowest angles (0º). That means the composite (HA/AL_2O_3) has an important effect on adsorption and wetting behavior. Fig. 10 shows the contact angle of the coating layer. Wettability of Surface is very significant in the case of an implant that is placed inside the human body and must should be hydrophilic when the contact angle is greater than 90º. It favors interactions with biological fluids and cells when compared to hydrophobic ones. In this study, excellent stage of super hydrophilic has been reached. the contact angle reached

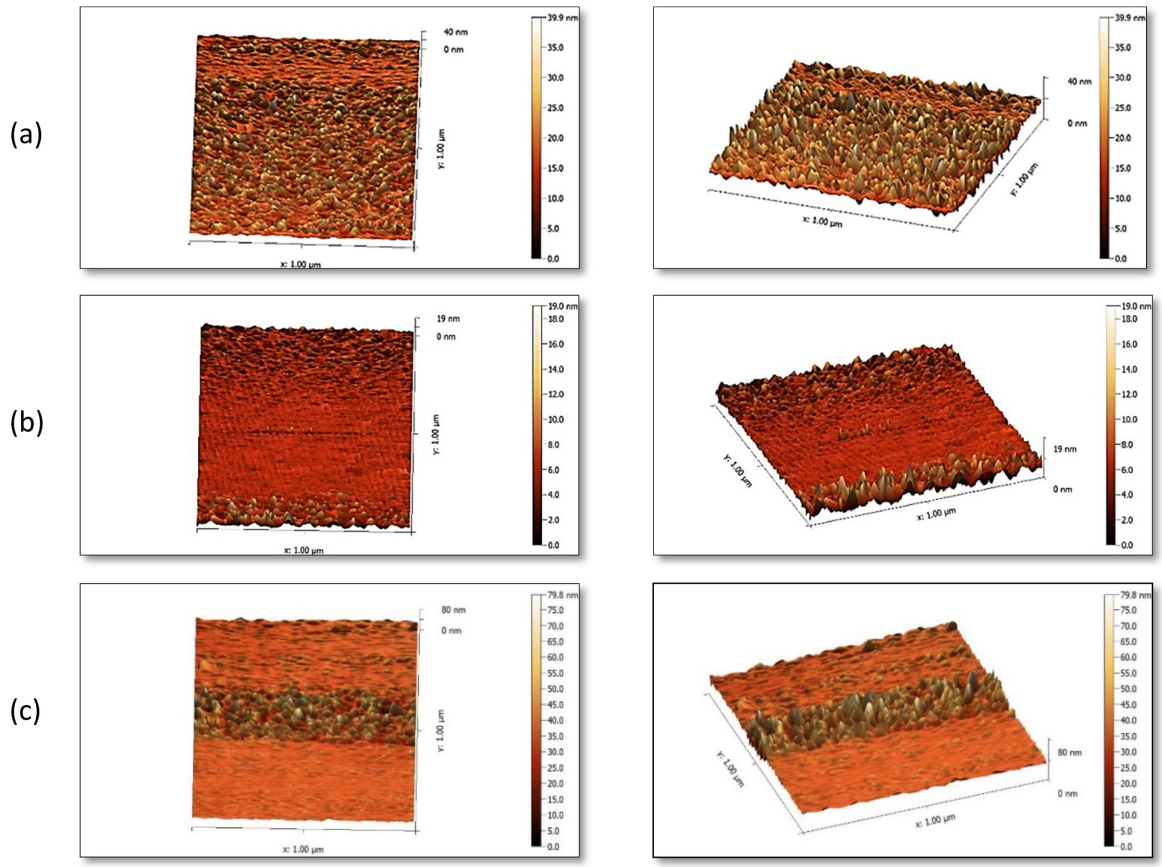

Fig. 8. Two and three dimensions features of (AFM) images for (a) one-layer BG, (b) one-layer Composite ($HA+Al_2O_3$), and (c) Three-layer (BG+ Composite +BG) coating samples

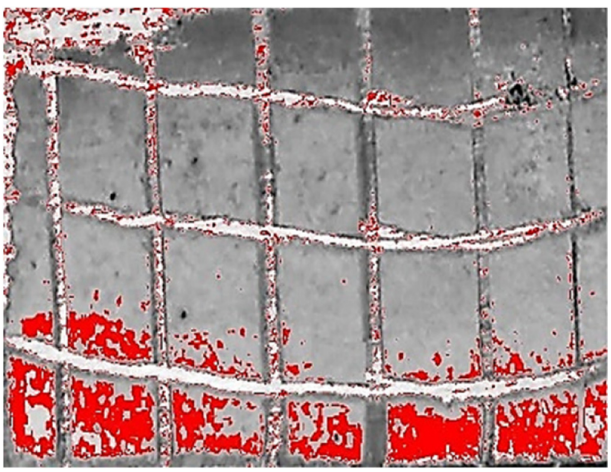

Fig. 9. Optical image for deposited coating of Three-layer (BG+ Composite +BG) coating sample

to its lowest value 0°.

A large number of studies have found that cells preferred to attach and spread on hydrophilic surfaces as compared over hydrophobic [16]. Moreover, the super hydrophilic property represented by sample Three layer (BG+ Composite +BG) This is probably because the alumina surface has extreme hydrophilic characteristics [8,23,24].

Table 7. the removal area of the three samples

NO.	Type of sample	Removal area %
1	one-layer BG	11.33
2	one-layer Composite ($HA+Al_2O_3$)	7.59
3	Three layers (BG+ Composite +BG)	11.92

4.6 Antibacterial assessment

Staph. and E. coli were chosen to represent gram-positive and gram-negative respectively. So, the two group of the coating tests samples are used. Each group of samples was immersed in a type of bacteria. The first group was immersed in Staph bacteria and the second group was immersed in E. coli bacteria. Fig. 11 shows

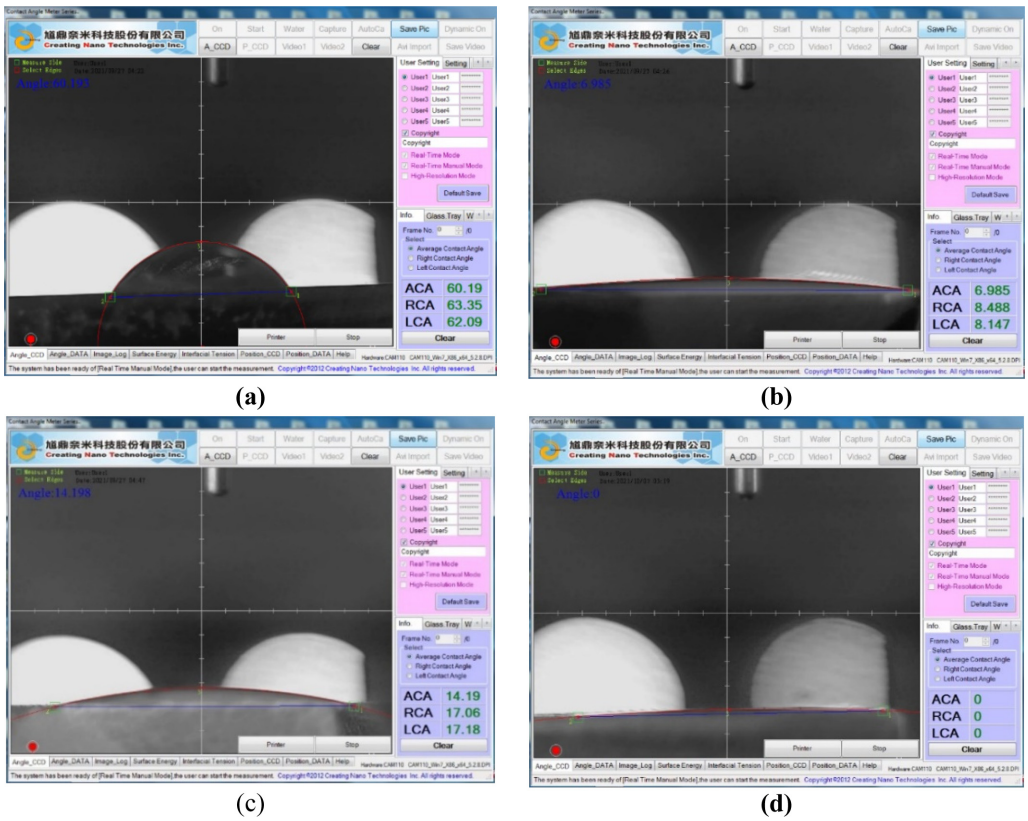

Fig. 10. contact angle of the coating layer test (a) Substrate, (b) one-layer BG, (c) one-layer Composite ($HA+Al_2O_3$), (d) Three layer (BG + Composite + BG)

Table 8. The measurement of contact angle for different samples

NO.	Type of sample	Contact angle (°)
1	substrate	60.19
2	one-layer BG	6
3	one-layer Composite ($HA+Al_2O_3$)	14
4	Three layers (BG+ Composite +BG)	0

image of the samples for Staphylococcus aureus (gram positive) and E. coli (gram negative), shows inhibition zone for antimicrobial coating. The clear zone formation around the disc indicates the bacterial inhibition.

Table 9 shows the measured inhibition zone for antimicrobial coating composition of two types of bacteria, Staphylococcus aureus and E. coli. The substrate shows no change in the surrounding bacterial concentration at all. whereas other samples show good antimicrobial activities.

The results show that the antimicrobial activity of 45S5 bioglass particles inhibits S. aureus (Gram positive) and E. coli (Gram negative) (37and 55) mm respectively., but a higher level of inhibition was observed with E. coli. The presence of (Gram positive) S. aureus and bioglass particals(which have a negative surface charge) will lead to good adhesion of bacteria on bioglass particals, but the sharp glass debris will damage bacterial cell walls, thus creating hollows and holes on the cell wall and facilitating the penetration of antimicrobial agents into the microbial cytoplasm [17,25].

In addition, E. coli has an outer membrane infused with pore proteins. The 45S5 Bioglass particles produce dissolved products, namely sodium (Na) and calcium (Ca) ions, which are of a tiny enough size to permeate into these proteins. Once inside, they raise the intracellular pH, leading to the demise of the cells. Increased pH values in the medium may modify the pH gradient in the cytoplasmic membrane of bacteria, which is crucial for transporting nutrients into the cell. Consequently, the elevated pH might hinder the movement and ability of the cytoplasmic membrane, leading to suppression and harmful consequences for the bacteria, ultimately causing damage to their structure [17,26].

Table 9. shows measured inhibition zone for antimicrobial coating composition of two types of bacteria Staphylococcus aureus and E. coli

NO.	Type of sample	Zone of inhibition in Staph (mm)	Zone of inhibition in E. coli (mm)
1	substrate	0	0
2	one-layer BG	37	55
3	one-layer Composite (HA+Al_2O_3)	32	33
4	Three layers (BG+ Composite +BG)	35	33

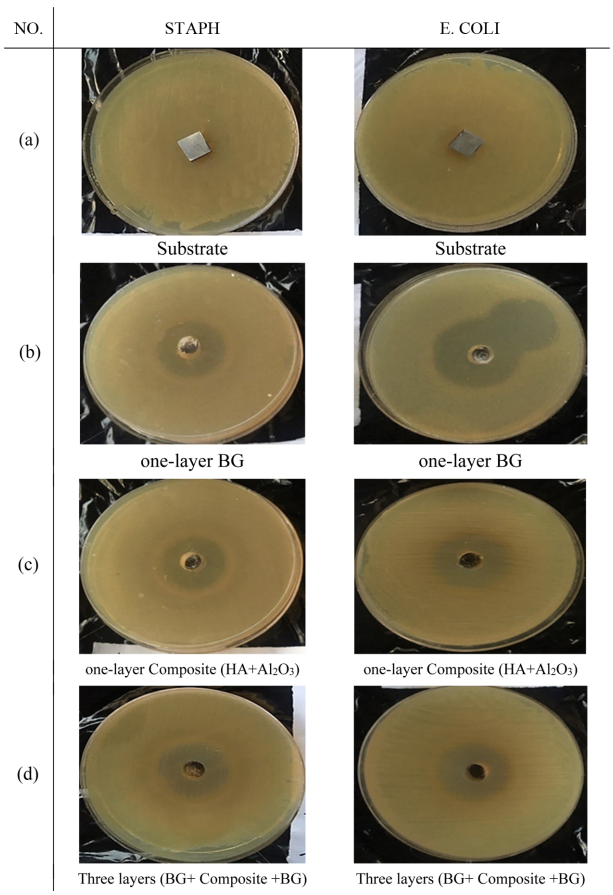

Fig. 11. Shows images for staph. and E. coli bacteria by well diffusion method (a) substrate (b) one-layer BG, (c) one-layer Composite, (d) Three-layer (BG+ Composite +BG) coating samples

One- layer composite (HA+ Al_2O_3) has an inhibition zone of (32 and 33) mm for staph and E.coli respectivly. Three-layers sample (BG+ composite + BG) was tested for their antimicrobial activities and measured using their zone of inhibition against Staph. E. coli were (38 and 36) mm respectively. These results indicated that the existence of Al_2O_3 had decreased the antibacterial activity of 45S5 bioactive glasses, but the Al_2O_3 was used due to their good mechanical properties. The interaction between bacteria and biomaterial surfaces has multiple aspects properties that must be considered, including surface energy, wettability, surface charges, entrapped air and surface topography, as well as particle concentration, shape and size. Moreover, the shape and size of bacteria also play a role in bacterial interactions with material surfaces.

Moreover, during the antibacterial test, the alumina inhibited the BG antibacterial effect. That means that even though we used 5% Al_2O_3 as a deposit condition, the effect of $Al_2O_3$was observed. From the antibacterial test, BG coated surface with 5% Al_2O_3 showed the good antibacterial activity.

4.7 Biomimetic test

The bioactivity of the coating is crucial for guaranteeing the successful integration of the bone implant in real-life situations. To assess this, samples were tested: (BG) and (BG+ Composite +BG), which were immersed in SBF to evaluate their bioactivity.

These samples have been divided into three groups each group was immersed in the SBF for 5 days, 1 week, and 2 weeks. Furthermore, the bioactivities of different coatings have been determined using optical microscopy.

It was used to study the morphology of the coating after immersion in the SBF, Fig. 12 uncoated substrate's surface were covered with small apatite particles when immersion in SBF.

The Fig. 12 alliterated optical microscopy images for (a) one layer (BG), and (b) three layers (BG+ Composite +BG), after 5 days', 1 week and 2 weeks' immersion in simulation body flowed (SBF). The findings demonstrated that the surface of the coated substrate, both in the one-layer (BG) sample and the three layers (BG+ Composite +BG), exhibited the formation of hydroxy carbon apatite (HCP), as seen in Fig. 13.

The findings suggest that the presence of alumina at the given concentration did not noticeably impact the

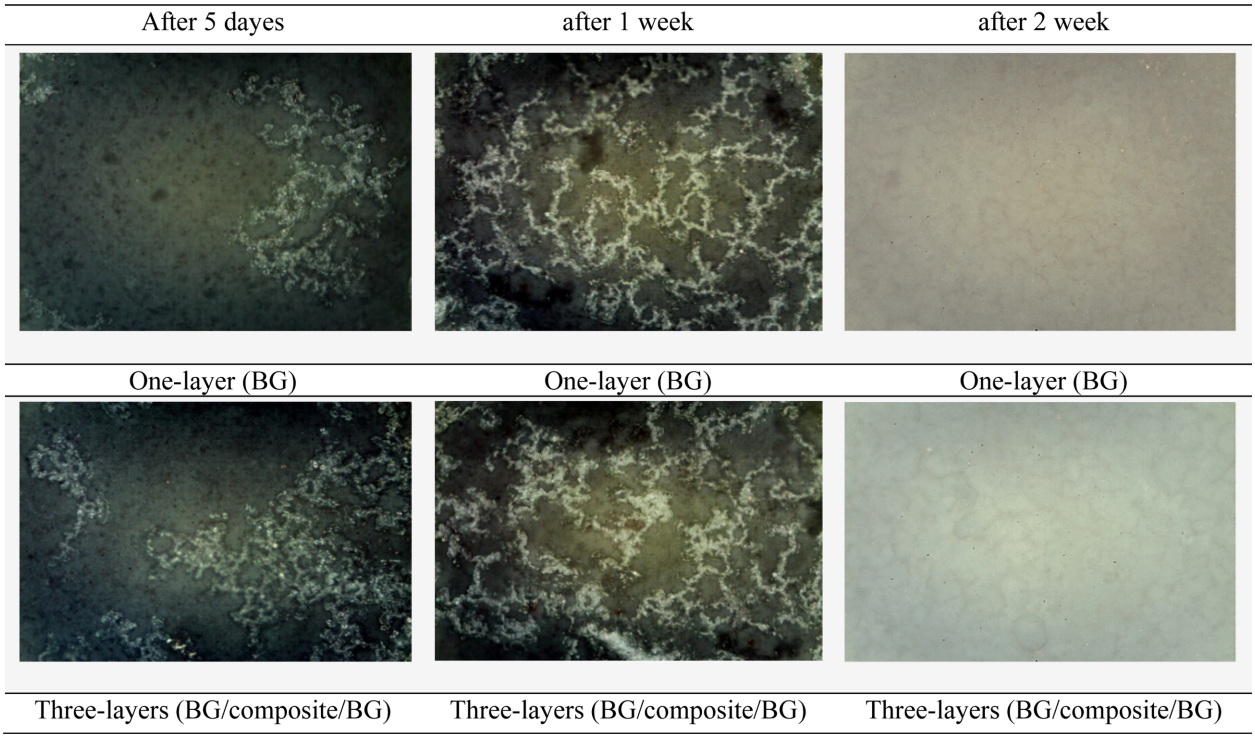

Fig. 12. Optical microscopy images for (a) one –layer (BG), and (b)three layers (BG+ Composite +BG), after 5 days, 1 week and 3 weeks of immersion in SBF

inhibition of apatite formation. It is essential to mention that applying a substantial quantity of Bioglass® particles increases bioactivity [18].

Extending the immersion period to two weeks, the surface became covered entirely with small and large apatite particles. Additionally, these particles were noticeably clustered due to increased apatite nucleation.

This suggests the formation of a layer of apatite on the surface, which is characteristic of mineralized bio ceramic materials. It should be noted that the uncoated substrate's surface showed high biocompatibility, as shown in Fig. 13, where covered with small apatite particles when immersed in SBF.

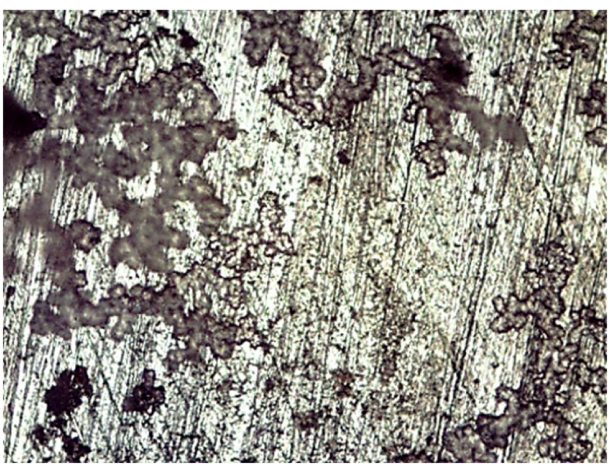

Fig. 13. uncoated substrate's surface were covered with small apatite particles when immersion in SBF

4.8 Corrosion behavior of the coating

The polarization curves regarding Co-Cr-Mo alloy with and without coatings in the SBF' solution at 37 ºC, Co-Cr-Mo alloy without coating, one-layer BG, composite (HA/Al_2O_3), one layer, and Three-layer (BG+ Composite +BG) coating samples are shown in Fig. 14. The coated Co-Cr-Mo alloy was significantly changed to a low current density, indicating great resistance to corrosion. The coated Co-Cr-Mo alloy has enhanced corrosion resistance compared to the Co-Cr-Mo alloy, as shown by lower anodic current densities.

The study showed that the Co-Cr-Mo alloy specimens with a coating had exceptional resistance to corrosion in the SBF solution. Table 8 contains the parameters for corrosion characteristics that are obtained from cyclic curves.

The corrosion of coated samples with one-layer BG,

Table 10. Results of electrochemical corrosion parameters following corrosion testing on all layers upon immersion in SBF

NO.	Type of sample	I_{pitt}	E_{pitt}
1	Substrate	2.15372	627.17
2	one-layer BG	1.13977	810.815
3	one-layer Composite (HA+Al_2O_3)	0.507309	399
4	Three layers (BG+ Composite +BG)	0.03956	999.85

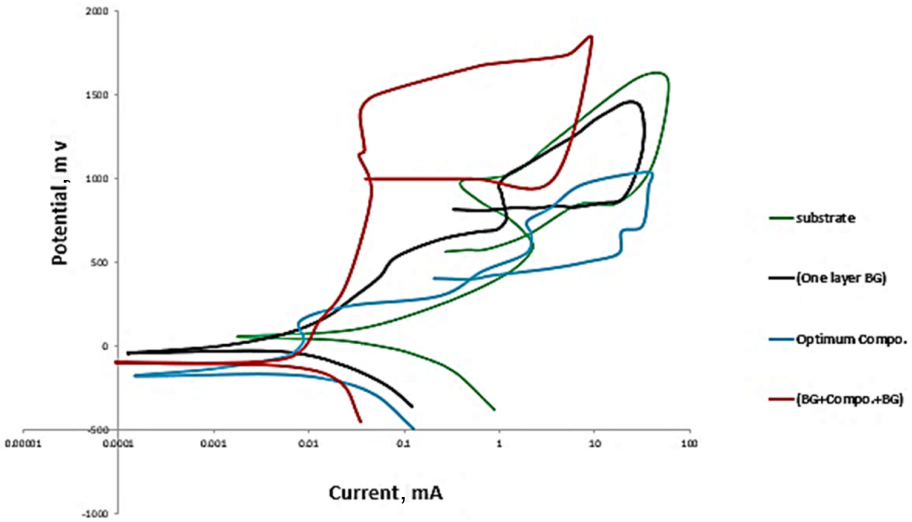

Fig. 14. cyclic polarization potentiodynamic test (CPPT) for, substrate, one-layer BG, one-layer Composite, and Three layer (BG+ Composite +BG) immersed in SBF solution 37°C coating samples

composite (HA/Al_2O_3), and Three-layer (BG+ Composite +BG) coating samples is significantly reduced. The passivation voltages (E_{pit}) and (I_{Pitt}), as well as the current,

Table 11. Cr ion release of coating samples

NO.	Type of sample	Cr Ion Release for five weeks (ppm)
1	substrate	0.83
2	one-layer BG	0.13
3	one-layer Composite (HA+Al_2O_3)	0.65
4	Three layers (BG+ Composite +BG)	0.04

for Co-Cr-Mo uncoated, one-layer BG, composite (HA/Al_2O_3), one layer, and three layers (BG+ Composite +BG), are shown in Fig. 14. The whole set of values for the outcome can be seen in Table 10.

The presence of pitting corrosion was verified by observing the corrosion of the sample and identifying the specific kind of corrosion taking place. The barking down of the oxide layer and the next re-passivation for the coated samples indicate that these coatings have a self-healing ability.

The (BG+ Composite +BG) coating caused a change in the diagram towards lower corrosion current density values and more noble potentials. This indicates that the

Table 12. Porosity thickness and Cr ion release of coating samples

NO.	Type of sample	Cr Ion Release for five weeks (ppm)	Thickness
1	substrate	0.83	
2	one-layer BG	0.13	80
3	one-layer Composite (HA+Al_2O_3)	0.65	17
4	Three layers (BG+ Composite +BG)	0.04	177

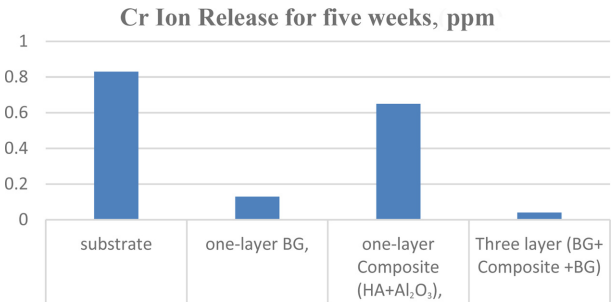

Fig. 15. Cr ion released in 0.9% NaCl for samples at four weeks

coating successfully achieved high corrosion resistance by reducing the corrosion rate of the Co-Cr-Mo alloy substrate in the SBF solution [27,28].

4.9 Chromium Ion release measurements

Each sample's chromium concentration emitted per unit surface area is measured in parts per billion (ppb). Table 11 and Fig. 15 display the Cr ion content of several samples immersed in a 0.9% NaCl solution for five weeks. The samples include a substrate, one-layer BG, one-layer composite, and three-layer (BG + Composite + BG) coatings. The released Cr ion content for these samples at five weeks is as follows: 0.83 ppm for substrate, 0.13 ppm for one-layer BG, 0.65 ppm for one-layer composite, and 0.04 ppm for three-layer (BG + Composite + BG) coating. It was observed that the release of chromium ions is more pronounced on the substrate. However, when it comes to coating samples, the release of Cr ions is lower in comparison to the substrate.

It can be seen from the result of the It can be observed from Table 12 that the amount of Cr ion release decreases with the increasing of thickness. Furthermore, it is vital to acknowledge that porosity has a significant effect. This is because the porosity exposes the surface of the samples to a 0.9% NaCl solution, resulting in a substantial release of ions. These coatings serve as a protective barrier against Cr oxidation and alter the oxidation process of Cr, preventing the release of Cr ions into the immersion solution.

5. Conclusion

- High thickness was achieved by EPD was used to deposit factional graded the three layers (BG+ Composite +BG).
- Three layers (BG+ Composite +BG) exhibited the formation of hydroxycarbon apatite (HCP) the presence of alumina at the used concentration did not noticeably impact the inhibition of apatite formation.
- The coating show high bioactivity in the biomimetic test since the HCP was initiated in 5 days.
- During the wettability test the alumina made the coated sample (BG+ Composite +BG), super hydrophilic (CA=0).
- Moreover, during the antibacterial test, the alumina inhibited the BG antibacterial effect.
- That means that even though we used 5% Al_2O_3 as a deposit condition, the effect of Al_2O_3 was observed.
- In the Cr release, show a significant drop in the released Cr after substrate coating, especially in three-layer (BG+ Composite +BG).
- This indicates that the coating successfully achieved high corrosion resistance by reducing the corrosion rate of the Co-Cr-Mo alloy substrate in the SBF solution.

References

1. S. Tharani Kumar, S. Prasanna Devi, C. Krithika, and R. N. Raghavan, Review of Metallic Biomaterials in Dental Applications, *Journal of Pharmacy & Bioallied Sciences*, **12**, S14 (2020). Doi: https://doi.org/10.4103/JPBS.JPBS_88_20
2. Joël Fauré, Richard Drevet, Sylvain Potiron, Doina Margareta Gordin, Hassane Oudadesse, Thierry Gloriant, and Hicham Benhayoune, Electrophoretic deposition of bioactive glass coatings on Ti12Mo5Ta alloy, *Key Engineering Materials*, **507**, 135 (2012). https://doi.org/10.4028/www.scientific.net/KEM.507.135
3. L. L. Hench, *An Introduction to Bioceramics 2nd ed.*, pp. 71 - 85, World Scientific Publishing Co Pte Ltd., Singapore (2013). Doi: https://doi.org/10.1142/9781908977168_0004
4. F. Baino, S. Ferraris, M. Miola, E. Verné, I. Evans, and O. Bretcanu, *Biomedical, Therapeutic and Clinical Applications of Bioactive Glasses*, pp. 35 – 67, Woodhead Publishing, UK (2018). Doi: https://doi.org/10.1016/B978-0-08-102196-5.00002-1
5. Marwan B. Hussein, Ali M. Mustafa, Makarim H. Abdulkareem, and Ahmed A. Alamiery, Comparative corrosion performance of YSZ-coated Ti-13Zr-13Nb alloy

and commercially pure titanium in orthopedic implants, *South African Journal of Chemical Engineering*, **48**, 40 (2024). Doi: https://doi.org/10.1016/j.sajce.2024.01.005

6. E. Denes, G. Barrière, E. Poli, and G. Lévêque, Alumina biocompatibility, *Journal of Long-Term Effects of Medical Implants*, **28**, 9 (2018). Doi: https://doi.org/10.1615/JLongTermEffMedImplants.2018025635
7. X. Q. Zhang, L. H. Yin, M. Tang, and Y. P. Pu, ZnO, TiO_2, SiO_2, and Al_2O_3 nanoparticles-induced toxic effects on human fetal lung fibroblasts, *Biomedical and Environmental Sciences*, **24**, 661 (2011). Doi: https://doi.org/10.3967/0895-3988.2011.06.011
8. K. Ishikawa, S. Matsuya, Y. Miyamoto, and K. Kawate, 9.05 - Bioceramics, *Comprehensive Structural Integrity*, **9**, 169 (2007). Doi: https://doi.org/10.1016/B0-08-043749-4/09146-1
9. Marwan B. Hussein, Ali M. Mustafa, and Makarim H. Abdulkareem, A Comparative Study on Dip Coating and Corrosion Behavior of Ti-13Zr-13Nb and Commercially Pure Titanium Alloys Coated with YSZ by Taguchi Design, *Salud, Ciencia y Tecnología-Serie de Conferencias*, **3**, 847 (2024). Doi: https://doi.org/10.56294/sctconf2024847
10. T. Moskalewicz, A. Kukaszczyk, A. Kruk, M. Kot, D. Jugowiec, B. Dubiel, A. Radziszewska, Porous HA and nanocomposite nc-TiO2/HA coatings to improve the electrochemical corrosion resistance of the Co-28Cr-5Mo alloy, *Materials Chemistry and Physics*, **199**, 144 (2017). Doi: https://doi.org/10.1016/j.matchemphys.2017.06.064
11. M. Mehdipour, A. Afshar, and M. Mohebali, Electrophoretic deposition of bioactive glass coating on 316L stainless steel and electrochemical behavior study, *Applied Surface Science*, **258**, 9832 (2012). Doi: https://doi.org/10.1016/J.APSUSC.2012.06.038
12. L. Besra and M. Liu, A review on fundamentals and applications of electrophoretic deposition (EPD), *Progress in Materials Science*, **52**, 1 (2007). Doi: https://doi.org/10.1016/j.pmatsci.2006.07.001
13. F. M. Klenke, Y. Liu, H. Yuan, E. B. Hunziker, K. A. Siebenrock, and W. Hofstetter, Impact of pore size on the vascularization and osseointegration of ceramic bone substitutes in vivo, *Journal of Biomedical Materials Research A*, **85**, 777 (2008). Doi: https://doi.org/10.1002/JBM.A.31559
14. K. A. Hing, S. M. Best, and W. Bonfield, Characterization of porous hydroxyapatite, *Journal of Materials Science: Materials in Medicine*, **10**, 135 (1999). Doi: https://doi.org/10.1023/A:1008929305897
15. M. Śmiga-Matuszowicz, B. Janicki, K. Jaszcz, J. Kukaszczyk, M. Kaczmarek, M. Lesiak, A. L. Sieroń, W. Simka, M. Mierzwiński, D. Kusz, Novel bioactive polyester scaffolds prepared from unsaturated resins based on isosorbide and succinic acid, *Materials Science and Engineering C*, **45**, 64 (2014). Doi: https://doi.org/10.1016/J.MSEC.2014.08.069
16. K. Webb, V. Hlady, and P. A. Tresco, Relative importance of surface wettability and charged functional groups on NIH 3T3 fibroblast attachment, spreading, and cytoskeletal organization, *Journal of Biomedical Materials Research*, **41**, 422 (1998) Doi: https://doi.org/10.1002/(sici)1097-4636(19980905)41:3<422::aid-jbm12>3.0.co;2-k
17. S. Begum, W. E. Johnson, T. Worthington, and R. A. Martin, The influence of pH and fluid dynamics on the antibacterial efficacy of 45S5 Bioglass, *Biomedical Materials*, **11**, 15006 (2016). Doi: https://doi.org/10.1088/1748-6041/11/1/015006
18. F. Pishbin, A. Simchi, M. P. Ryan, and A. R. Boccaccini, Electrophoretic deposition of chitosan/45S5 Bioglass® composite coatings for orthopaedic applications, *Surface and Coatings Technology*, **205**, 5260 (2011). Doi: https://doi.org/10.1016/j.surfcoat.2011.05.026
19. A. M. Mustafa, F. F. Sayyid, N. Betti, L. M. Shaker, M. M. Hanoon, A. A. Alamiery, A. A. H. Kadhum, and M. S. Takriff, Inhibition of mild steel corrosion in hydrochloric acid environment by 1-amino-2-mercapto-5-(4-(pyrrol-1-yl) phenyl)-1, 3, 4-triazole, *South African Journal of Chemical Engineering*, **39**, 42 (2022). Doi: https://doi.org/10.1016/j.sajce.2021.11.009
20. A. M. Mustafa, F. F. Sayyid, N. Betti, M. M. Hanoon, Ahmed Al-Amiery, A. A. H. Kadhum, and M. S. Takriff, Inhibition Evaluation of 5-(4-(1H-pyrrol-1-yl) phenyl)-2-mercapto-1, 3, 4-oxadiazole for the Corrosion of Mild Steel in an Acidic Environment: Thermodynamic and DFT Aspects, *Tribologia Finnish Journal of Tribology*, **38**, 39 (2021). Doi: https://doi.org/10.30678/fjt.105330
21. A. K. Khudhair, A. M. Mustafa, M. M. Hanoon, A. Al-Amiery, L. M. Shaker, T. Gazz, A. B. Mohamad, A. H. Kadhum, and M. S. Takriff, Experimental and theoretical investigation on the corrosion inhibitor potential of N-MEH for mild steel in HCl, *Progress in Color, Colorants and Coatings*, **15**, 111 (2022). Doi: https://doi.rog/10.30509/PCCC.2021.166815.1111
22. Mustafa, A. M., Z. S. Abdullahe, F. F. Sayyid, M. M. Hanoon, A. A. Al-Amiery, and W. N. R. W. Isahak, 3-

Nitrobenzaldehyde-4-phenylthiosemicarbazone as Active Corrosion Inhibitor for Mild Steel in a Hydrochloric Acid Environment, *Progress in Color, Colorants and Coatings*, **15**, 285 (2022). Doi: https://doi.org/10.30509/pccc.2021.166869.1127

23. Firas F. Sayyid, Ali M. Mustafa, Mahdi M. Hanoon, Lina M. Shaker, and Ahmed A. Alamiery, Corrosion Protection Effectiveness and Adsorption Performance of Schiff Base-Quinazoline on Mild Steel in HCl Environment, *Corrosion Science and Technology*, **21**, 77 (2022). Doi: https://doi.org/10.14773/cst.2022.21.2.77
24. A. N. Jasim, A. Mohammed, A. M. Mustafa, F. F. Sayyid, H. S. Aljibori, W. K. Al-Azzawi, A. A. Al-Amiery, and E. A. Yousif, Corrosion Inhibition of Mild Steel in HCl Solution by 2-acetylpyrazine: Weight Loss and DFT Studies on Immersion Time and Temperature Effects, *Progress in Color, Colorants and Coatings*, **17**, 333 (2024). Doi: https://doi.org/10.30509/PCCC.2024.167231.1261
25. I. A. Annon, K. K. Jlood, N. Betti, T. S. Gaaz, M. M. Hanoon, F. F. Sayyid, A. M. Mustafa, and A. A. Alamiery, Unlocking corrosion defense: investigating Schiff base derivatives for enhanced mild steel protection in acidic environments, *International Journal Corros. Scale Inhib.*, **13**, 727 (2024). Doi: https://doi.org/10.17675/2305-6894-2024-13-2-5
26. Firas F. Sayyid, Ali M. Mustafa, Slafa I. Ibrahim, Mahdi M. Hanoon, A. A. H. Kadhum, W. N. R. W. Isahak, and A. A. Al-amiery, Gravimetric Measurements and Theoretical Calculations of 4-Aminoantipyrine Derivatives as Corrosion Inhibitors for Mild Steel in Hydrochloric Acid Solution: Comparative Studies, *Corrosion Science and Technology*, **22**, 73 (2023). Doi: https://doi.org/10.14773/cst.2023.22.2.73
27. M. K. Abbass, K. M. Raheef, I. A. Aziz, M. M. Hanoon, A. M. Mustafa, W. K. Al-Azzawi, A. A. Al-Amiery, and A. A. H. Kadhum, Evaluation of 2-Dimethylaminopropionamidoantipyrine as a Corrosion Inhibitor for Mild Steel in HCl Solution: A Combined Experimental and Theoretical Study, *Progress in Color, Colorants and Coatings*, **17**, 1 (2024). Doi: https://doi.org/10.30509/PCCC.2023.167134.1216
28. M. Taha Mohamed, S. A. Nawi, A. M. Mustafa, F. F. Sayyid, M. M. Hanoon, A. A. Al-Amiery, A. A. H. Kadhum, and W. K. Al-Azzawi, Revolutionizing Corrosion Defense: Unlocking the Power of Expired BCAA, *Progress in Color, Colorants and Coatings*, **17**, 97 (2024). Doi: https://doi.org/10.30509/PCCC.2023.167156.1228
29. A. A. Zainulabdeen, Z. A. Betti, D. M. Jamil, A. M. Mustafa, F. F. Sayyid, M. M. Hanoon, T. S. Gaaz and A. Alamiery, Inhibition mechanism and corrosion protection of mild steel in hydrochloric acid using 2-hydroxynaphthaldehyde thiosemicarbazone (2HNT): Experimental and theoretical analysis, *International Journal of Corrosion and Scale Inhibition*, **13**, 935 (2024). Doi: https://doi.org//10.17675/2305-6894-2024-13-2-16